Title: Identification of the binding site of apical membrane antigen 1 (AMA1) inhibitors using a paramagnetic probe

Authors: MANSURA AKTER; Nyssa Drinkwater; Shane M. Devine; Simon C. Drew; Krishnarjuna Bankala; Cael O. Debono; Geqing Wang; Martin J. Scanlon; Peter J. Scammells; Sheena McGowan; Christopher A. MacRaild; Raymond S. Norton

To be cited as: 10.1002/cmdc.201800802

Link to VoR: https://doi.org/10.1002/cmdc.201800802

Identification of the binding site of apical membrane antigen 1 (AMA1) inhibitors using a paramagnetic probe

Mansura Akter,[a] Nyssa Drinkwater,[b] Shane M. Devine,[a] Simon C. Drew,[c] Krishnarjuna Bankala,[a] Cael O. Debono,[a] Geqing Wang,[a] Martin J. Scanlon,[a] Peter J. Scammells,[a] Sheena McGowan,[b] Christopher A. MacRaild[a]* and Raymond S. Norton[a]*

[a] Medicinal Chemistry, Monash Institute of Pharmaceutical Sciences, Monash University, Parkville, Victoria 3052, Australia

[b] Biomedicine Discovery Institute, Department of Microbiology, Monash University, Wellington Rd, Clayton, Victoria 3800, Australia

[c] Department of Medicine (Royal Melbourne Hospital), The University of Melbourne, Melbourne, Victoria 3010, Australia

*Correspondence:
Christopher A. MacRaild
E-mail: chris.macraild@monash.edu
Raymond S. Norton
E-mail: ray.norton@monash.edu

Abstract

Apical membrane antigen 1 (AMA1) is essential for the invasion of host cells by malaria parasites. Several small-molecule ligands have been shown to bind to a conserved hydrophobic cleft in *Plasmodium falciparum* AMA1. However, a lack of detailed structural information on the binding pose of these molecules has hindered their further optimisation as inhibitors. We have developed a spin-labelled peptide based on RON2, the native binding partner of AMA1, to probe the binding sites of compounds on *Pf*AMA1. The crystal structure of this peptide bound to *Pf*AMA1 shows that it binds at one end of the hydrophobic groove, leaving much of the binding site unoccupied and allowing fragment hits to bind without interference. In paramagnetic relaxation enhancement (PRE)-based NMR screening, the ^{1}H relaxation rates of compounds binding close to the probe were enhanced. Compounds experienced different degrees of PRE as a result of their different orientations relative to the spin-label while bound to AMA1. Thus, PRE-derived distance constraints can be used to identify binding sites and guide further hit optimisation.

Introduction

Malaria is a mosquito-borne infectious disease caused by parasites of several species of *Plasmodium*, amongst which *P. falciparum* and *P. vivax* pose the greatest threat to human health. The global disease burden caused by malaria increased through the 1990s owing to emerging resistance of the parasite against drugs and the spread of insecticide-resistant mosquitoes; this is illustrated by the re-emergence of the disease in areas that had been previously malaria-free.[1] Although remarkable progress has been made in controlling malaria since 2000,[1] malaria deaths stood at 435,000 in 2017, up from 429,000 in 2015, suggesting that this progress has been stalled in recent years.[2] This trend coincides with the spread of artemisinin resistance throughout South-East Asia, and there is serious concern that this will spread globally, including to Africa, where malaria prevalence is the highest.[3] Resistance to the most effective drugs to treat malaria, artemisinin[4] and its partner drugs,[5,6] threatens the efficacy of frontline combination therapies, thus compromising global efforts.[7] This highlights an urgent need for novel antimalarial therapeutics.[8]

Most apicomplexan parasites, including the causative agents of malaria, share a conserved host cell invasion machinery.[9] Apical membrane antigen protein 1 (AMA1), an integral membrane protein, is an important component of this machinery. AMA1 is released from the microneme of the parasite to its apical surface, where it interacts with its binding partner, rhoptry neck protein 2 (RON2), another parasite protein secreted and inserted into the host cell membrane during invasion.[10,11] The AMA1/RON2 complex forms part of a tight ring-like structure, called the moving junction, between the parasite apex and the host cell membrane, which enables the parasite to enter the host cell.[12–14] AMA1 presents a conserved hydrophobic cleft that is the binding site for RON2. Several studies have shown that anti-AMA1 antibodies, inhibitory peptides and other molecules targeting this hydrophobic cleft disrupt the AMA1-RON2 interaction, and are able to block the invasion process.[13–16] By mapping the residues of AMA1 and RON2 involved in the interaction and determining inhibitor binding poses, small inhibitory molecules targeting the conserved hydrophobic cleft can be designed as a basis for developing a new class of antimalarial.[17]

Previously, a fragment screen identified a range of small-molecule ligands for the conserved hydrophobic cleft of *Pf*AMA1.[18] Some of those AMA1 hits were tested in chemical shift perturbation assays and several sub-sites on AMA1 were identified, all of

which represent possible binding sites to be targeted in subsequent medicinal chemistry campaigns.[19]

However, the specific binding sites of these fragments remain elusive as there are no experimental details defining the binding pose(s) of these molecules in the hydrophobic cleft. Efforts to crystallise AMA1-small molecule complexes, other than with peptides, have been unsuccessful, and NMR studies gave a qualitative indication of the binding sites but no specific structural information owing to flat structure-activity relationship (SAR) data and promiscuous binding of some of these molecules.[20] Moreover, computational docking without experimental support does not provide reliable binding information because of the dynamic nature of AMA1 and the plasticity of the protein-protein interaction surface.[21] As a result, the process of SAR-guided lead optimisation of these fragments has been hindered.

We have, therefore, pursued an alternative approach to define the binding sites of elaborated fragments using paramagnetic relaxation enhancement (PRE). PRE is caused by magnetic dipolar interactions between a nucleus and the unpaired electron of a paramagnetic centre, for example, a spin label, and results in an increase in the relaxation rate of the nuclear magnetisation in a distance-dependent manner.[22,23] Spin labels such as nitroxide radicals are chemically stable, have a free electron, are paramagnetic and, owing to the large magnetic moment of an unpaired electron, exert detectable effects over distances up to 20-25 Å.[24,25] PRE methods have been used extensively for structural characterisation of protein and protein-ligand complexes where the protein itself is spin-labelled.[26–29] In fragment-based ligand design, a ligand with a defined binding site can be spin-labelled to search for second ligands that bind to adjacent sites.[30] Adopting this concept of second-site screening, here we describe the design, synthesis and application of a spin-labelled probe based on the C-terminal loop of the RON2 peptide[31] that would bind near the hydrophobic cleft of AMA1 and exert PRE effects on ligands bound nearby. Our designed peptide was based on a 13-residue truncated, disulfide-cyclised β-hairpin of RON2, RON2hp (CWTTRMSPPMQIC),[31] which, unlike longer RON2 signal peptides RON2sp1 or RON2sp2, makes extensive contacts with only one end of the hydrophobic cleft and leaves most of the cleft exposed. The disulfide bridge of RON2hp faces towards the centre of the hydrophobic cleft that has been identified as the primary hot spot for small molecule binding. To create a PRE probe, one of the disulfide-bridged Cys was substituted with D-Pro, which frees up the thiol group to allow spin-labelling. A crystal structure of the designed peptide bound to *Pf*AMA1 confirmed the expected binding site, and ligand-detected NMR studies using the probe showed that it was

able to provide useful information on the binding orientation of fragments bound to the hydrophobic cleft.

Results and Discussion

Design and development of the probe

The spin-labelled probe was designed based on the truncated 13-residue disulfide-bridged β-hairpin corresponding to the C-terminal loop of RON2, RON2hp[F2038W,Q2046M] (CWTTRMSPPMQIC) (Figure 1A).[31] Unlike the longer RON2sp1 peptide, RON2hp leaves most of the hydrophobic cleft free. The disulfide-bridge is positioned towards the centre of the hydrophobic cleft that has been identified as the primary hot spot for small molecule binding,[32] and thus offers an ideal site for Cys specific spin-labelling to confer PRE effects on molecules bound to the cleft. The highly conserved disulfide bridge between Cys2037 and Cys2049 helps stabilise an anti-parallel β-hairpin structure for the peptide.[33] Recent SAR studies on β-hairpin RON2 showed that a peptide with the disulfide bridge replaced by backbone linkers, for example, D-Pro-L-Pro, maintained binding affinity and functionality.[34] Initially, backbone-cyclised peptides were synthesised with either Cys2037 or Cys2049 substituted with D-Pro. The overall yields were 36% for both, with > 97% purity (Figure S1A). The backbone cyclisation efficiency was very high, with < 1% linear peptide remaining.

The binding affinities of the peptides were assessed using SPR for *P. falciparum* AMA1 from both FVO and 3D7 strains. As for native RON2hp, the peptides retained a slight preference for binding to FVO *Pf*AMA1 over 3D7 *Pf*AMA1 owing to an additional interaction with the polymorphic Asn225 residue.[31] The Cys2037-D-Pro2049 linked peptide bound to FVO *Pf*AMA1 with an affinity of 7 μM, whereas D-Pro2037-Cys2049 showed much weaker binding (Table 1). A 9-fold decrease in affinity for FVO *Pf*AMA1 from the parent peptide might arise from changes in local geometry around the disulfide bond. Therefore, further studies were carried on the Cys2037-D-Pro2049 cyclised peptide (bcRON2hp hereafter). A solution NMR study of the bcRON2hp peptide showed more than the expected 10 amide peaks, presumably because of *cis-trans* isomerisation of one or more of the three Pro residues (Figure S1B). This indicates that the peptide might adopt multiple conformations in solution, similar to the parent peptide.[31]

For the spin-labelled peptide, the free thiol group of Cys2037 of bcRON2hp specifically reacted with the thiosulfonate ester group of the MTSL spin label at neutral pH, with a final product yield of >95% and 100% purity (Figure S1C). The 1D ^{1}H spectrum of the spin-labelled peptide, N*bcRON2hp was characterised by extensive line broadening, with the most obvious effects on the Trp2038 indole peak adjacent to the MTSL-labelled Cys2037 (Figure S1D).

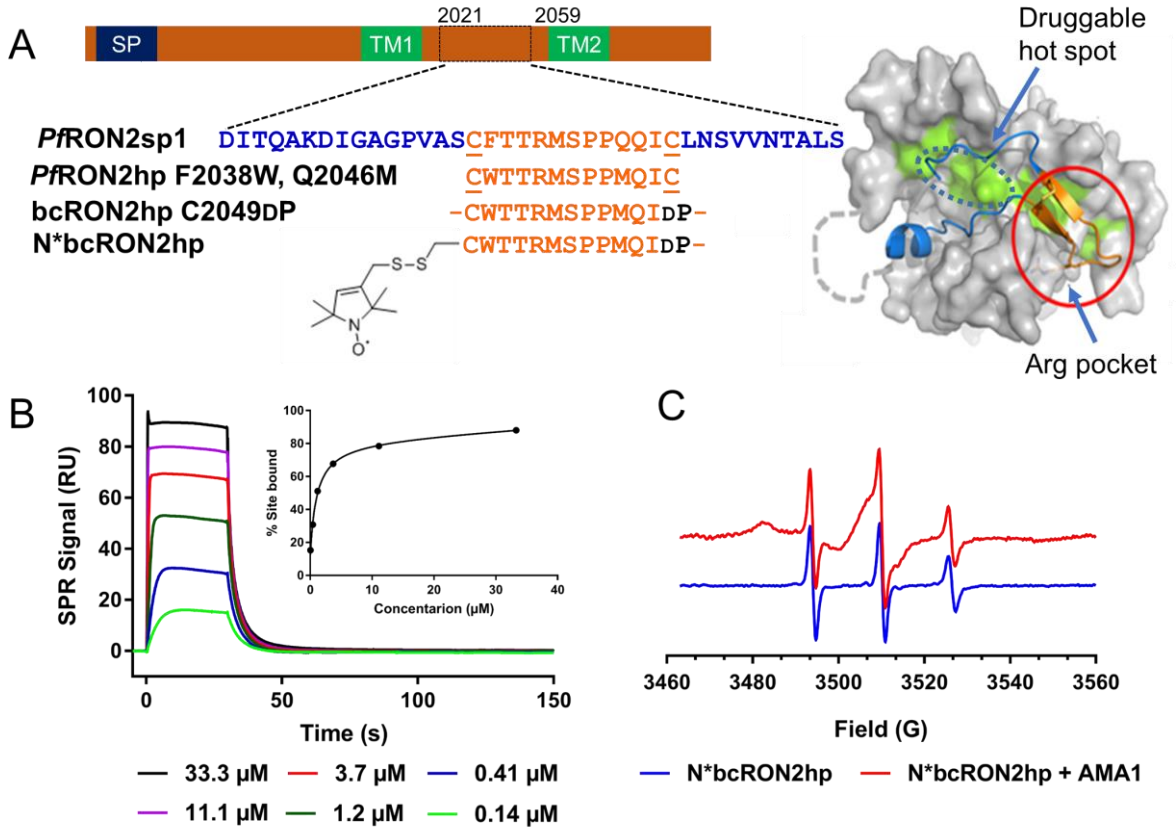

Figure 1. Design and development of the spin-labelled peptide as probe. A. Schematic overview of *Pf*RON2 protein. SP, signal peptide. TMD, putative membrane domain. Disulfide-bond-forming cysteines are underlined. The probe is designed based on the truncated RON2 hairpin RON2hp (orange) with two benefical mutations: Cys2049 is replaced with D-Pro and backbone cyclised with Cys2037 for bcRON2hp. The MTSL spin label is attached to the free -SH of Cys2037 of bcRON2hp. The residues involved in backbone cyclisation are hyphened. The right-hand panel shows the co-crystal structure of *Pf*AMA1 with *Pf*RON2sp1 peptide (PDB id: 3ZWZ)[35] reproduced from Wang et al.[31] *Pf*AMA1 is represented as grey surface. The hydrophobic cleft of AMA1 is highlighted in green with the druggable hot spot dashed circled and arrowed. The domain II loop of *Pf*AMA1 that is displaced on *Pf*RON2sp1 binding is depicted as a broken grey line. The β-hairpin of *Pf*RON2 (RON2hp, residues 2037-2049) coloured in orange and circled in red, binds to the polar Arg pocket (arrowed); the rest of the peptide is coloured in blue. B. SPR analysis of N*bcRON2hp binding to immobilized FVO *Pf*AMA1. C. First harmonic EPR spectra showing sharper line shape of N*bcRON2hp in the free state (blue), which broadens when bound to FVO *Pf*AMA1 (orange).

This confirmed that the nitroxide was in an active (oxidised state) electron spin state. Adding the MTSL spin-label moiety to the backbone-cyclised peptide slightly improved the affinity for FVO *Pf*AMA1 (2.2 μM) with respect to its unlabelled counterpart (Figure 1B, Table 1).

Table 1. Equilibrium dissociation constants (K_D) determined by SPR for the interaction of peptides with *Pf*AMA1.

Peptide	Sequence	FVO *Pf*AMA1 (K_D, μM)[a]	3D7 *Pf*AMA1 (K_D, μM)[a]
bcRON2hp, Cys2037D.Pro	DPWTTRMSPPMQIC	> 100	> 100
bcRON2hp, Cys2049D.Pro	CWTTRMSPPMQIDP	7.0 ± 0.8	15± 6
N*bcRON2hp	MTSL-CWTTRMSPPMQIDP	2.2 ± 0.5	33± 11
A_bcRON2hp	Acetyl-CWTTRMSPPMQIDP	5.8 ± 1	> 100

[a] Equilibrium dissociation constants (K_D) were estimated using a steady-state affinity algorithm available within the Biacore T200 evaluation program. The residues involved in backbone cyclisation are underlined. The data are expressed as mean ±standard error of the means (SEM) for experiments that were conducted on at least three independent occasions.

We noticed that N*bcRON2hp was reduced upon storage of the stock at 4 °C, resulting in approximately 2-5% diamagnetic impurity after four months owing to reduction of the nitroxide. This impurity will have little effect on the PRE calculation as the effect of the diamagnetic impurity is much weaker in the case of intermolecular PRE measurements on a complex with fast kinetics on the relaxation timescale.[36] Cys2037 of the unlabelled bcRONhp was also alkylated (Figure S1E) to prevent its intermolecular dimerization due to disulfide formation during storage and to serve as a diamagnetic control in screening experiments. The alkylated peptide, A_bcRON2hp retained affinity (5.8 μM) for FVO *Pf*AMA1.

Active electron spin of the probe in the bound state

To assess the oxidised state of the electron spin while bound to *Pf*AMA1, X-band EPR spectra of the peptide were recorded. The spectrum of free N*bcRON2hp exhibited sharp spectral line shapes (Figure 1C), characteristic of a single isotropically rotating component

with relatively fast motion.[27] Upon addition of FVO *Pf*AMA1, the signal broadened owing to binding of the N*bcRON2hp to AMA1. The broadened signal reflected a second well-defined component corresponding to the restricted motion expected for the AMA1-bound peptide, along with a sharp component arising from residual free peptide. Quantification of the spectra by double integration indicated that under these conditions, >90% of the peptide was bound to the protein, consistent with its affinity measured by SPR. The average electron "g factor" for the nitroxide radical was found to be 2.006, which is close to the "g" value for a free electron 2.003, indicating an intact spin. Numerical simulation of the EPR spectra indicated that the free spin-labelled peptide had a correlation time of 0.26 ns, consistent with a free small molecule undergoing isotropic rotation (Figure S2). The spin-labelled peptide bound to AMA1 had a correlation time of 8.4 ns, longer than the free peptide but surprisingly fast given that AMA1 (38 kDa) is expected to have a rotational correlation time of ~20 ns at 25 °C. This suggests that the nitroxide retains substantial flexibility in the complex. These data indicated that the nitroxide spin was oxidised and active in both free and AMA1-bound states. As expected, no EPR spectra were observed for the diamagnetic unlabelled bcRON2hp in both free and AMA1-bound states.

Crystal structure of N*bcRON2hp-AMA1 complex

The crystal structures of both unlabelled (bcRON2hp) and MTSL-labelled (N*bcRON2hp) peptides in complex with FVO *Pf*AMA1 were solved to define the probe binding mode and position of the spin label. Details of data collection and refinement are provided in Table 2. Purified recombinant FVO *Pf*AMA1 used for crystallisation eluted as a single peak in size-exclusion chromatography, consistent with the monomeric form of the protein (38 kDa) (Figure S3). The structures of bcRON2hp and N*bcRON2hp bound to FVO *Pf*AMA1, at 2.1 Å and 1.6 Å resolution respectively, showed that the designed peptides adopted a similar conformation and binding pose to the native peptide RON2hp,[31] and that the addition of the spin label had no effect on the overall position of the peptide. As expected, the peptides bound at one end of the hydrophobic cleft opposite to the DII loop, and interacted with the Arg pocket (Figure 2A). Overlay of the backbone-cyclised N*bcRON2hp and disulfide-cyclised RON2hp F2038W peptides (PDB id 4Z0D)[31] in the AMA1-bound structures revealed that the Cys2037-D-Pro2049 backbone constrained the N*bcRON2hp peptide structure sufficiently to adopt the native hairpin conformation stabilised by intra-molecular hydrogen bonds (Figure 2B, 2C). Thus, this scaffold positioned the side-chains of the key interacting residues Trp2038 and Arg2041 in an optimal orientation for binding to AMA1

(Figure 2D). An additional hydrophobic interaction with Tyr251 mediated by the nitroxide moiety of N*bcRON2hp might account for the improved affinity over its unlabelled counterpart (Figure 2D).

Table 2. Data collection and refinement statistics.

	FVO *Pf*AMA1- bcRON2hp	**FVO *Pf*AMA1-N*bcRON2hp**
PDB ID	6N7Q	6N87
Data Collection		
Wavelength (Å)	0.9537	0.9537
Resolution range (Å)	36.27 - 2.1 (2.175 - 2.1)[a]	40.79 - 1.588 (1.644 - 1.588)[a]
Space group	C 1 2 1	I 1 2 1
Unit cell	122.565 37.975 72.016 90 91.06 90	71.567 37.755 142.176 90 94.13 90
Total reflections	73917 (5980)	191591 (7829)
Unique reflections	19743 (1955)	51482 (4902)
Multiplicity	3.7 (3.8)	3.7 (3.4)
Completeness (%)	100.00 (100.00)	99.57 (95.87)
Mean I/sigma(I)	5.75 (1.53)	8.62 (1.42)
Wilson B-factor	19.92	14.25
R-pim (all I+ and I-)	0.124 (0.600)	0.056 (0.569)
CC1/2	0.984 (0.587)	0.997 (0.493)
Refinement statistics		
R-work	0.2069 (0.2726)	0.1604 (0.2708)
R-free	0.2428 (0.2973)	0.1882 (0.2967)
Number of non-H atoms	2351	2919
macromolecules	2187	2576
ligands		12
water	164	331
Protein residues	280	328
RMS(bonds)	0.003	0.016
RMS(angles)	0.62	1.38
Ramachandran favored (%)	96	97.46
Ramachandran allowed (%)		2.54
Ramachandran outliers (%)	0	0.00
Clashscore	1.19	3.61
Average B-factor	25.10	21.57
macromolecules	24.80	20.44
ligands		39.55
solvent	28.50	29.75

[a]Statistics for the highest-resolution shell are shown in parentheses.

Computational studies on AMA1 structures identified a druggable hydrophobic pocket (~420 Å^3 solvent-accessible volume) in the cleft as the primary hot spot for small molecule binding.[37,38] The pocket is surrounded by polar residues with a hydrophobic base composed of Ile252, Phe367 and Phe274, flanked by Tyr251 at one end and by Met273 at the other.[37] Again, the conformation adopted by 3D7 *Pf*AMA1 upon RON2sp1 binding (PDB id: 3ZWZ) revealed a pocket surrounded by Met224, Phe183, Tyr236 and Tyr251 in the centre of the hydrophobic cleft.[19] The N*bcRON2hp-FVO *Pf*AMA1 complex structure showed that in the bound state the nitroxide was oriented towards the druggable pocket sitting at the edge of the centre of the cleft (Figure 3).

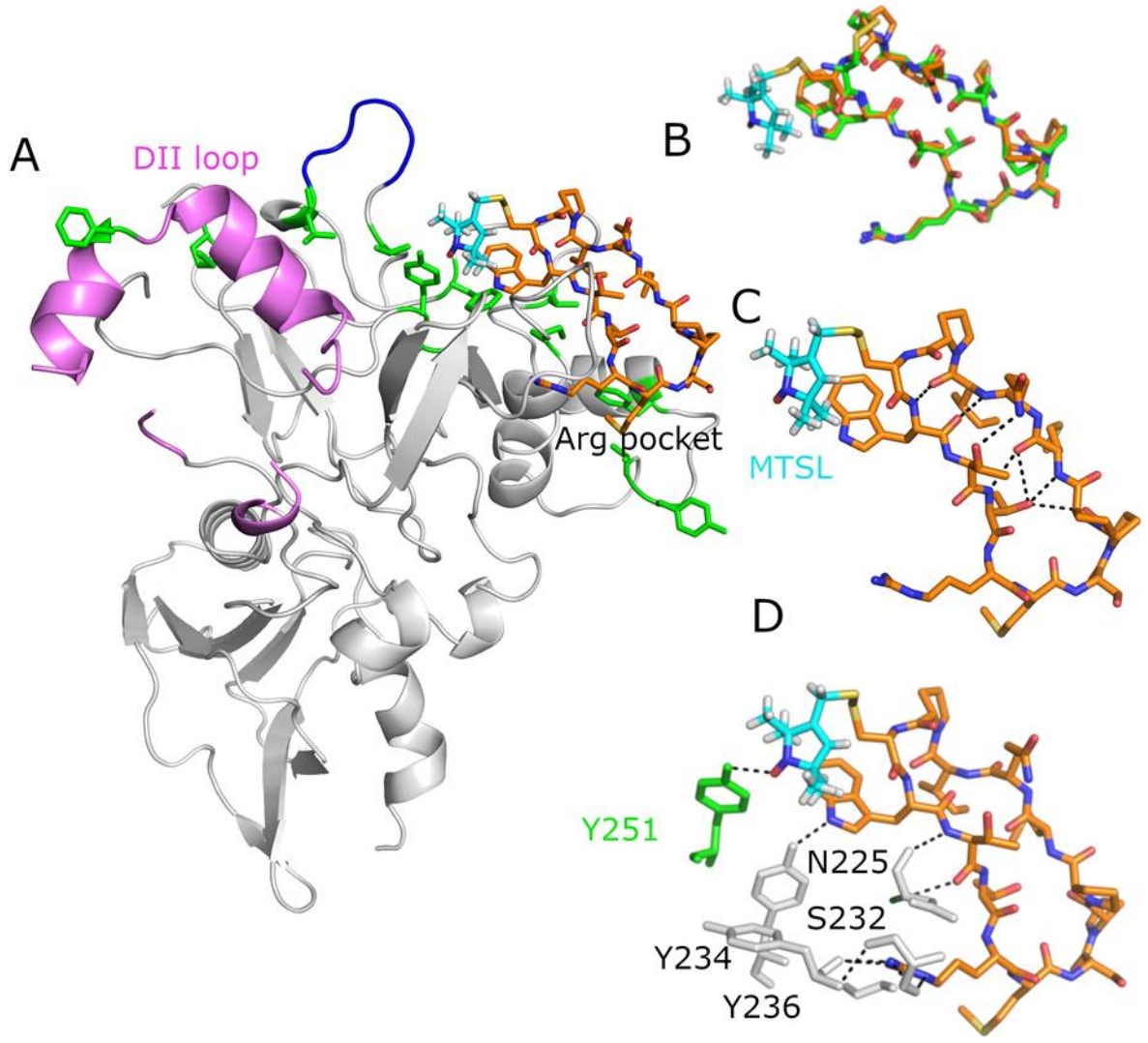

Figure 2. Crystal Structure of N*bcRON2hp complexed with FVO *Pf*AMA1. A. Cartoon representation of N*bcRON2hp-bound FVO *Pf*AMA1 structure. The spin-labelled peptide is situated at one end of the hydrophobic cleft, and occupies the polar Arg pocket opposite to the DII loop

(purple). The protein is shown in grey, conserved residues making the hydrophobic cleft in green sticks, and the domain Ib loop resolved in this structure in blue. The peptide is colored orange, with the MTSL moiety cyan. B. Structural alignment of N*bcRON2hp (orange) with native disulfide-bridged RON2hp (green). C. Intramolecular interactions within bound N*bcRON2hp constrained the peptide. D. Intermolecular interactions with AMA1; the spin label makes hydrophobic interactions with the conserved Tyr251 (green stick).

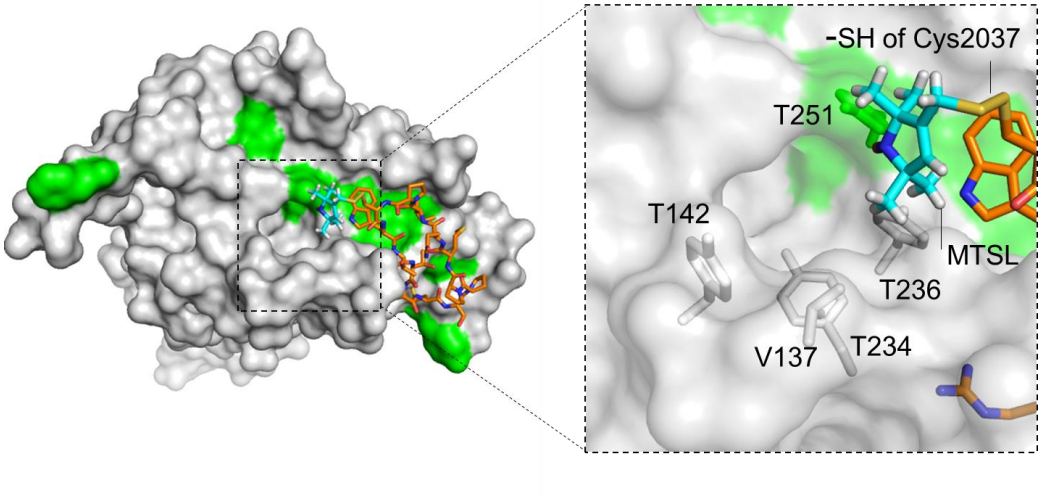

Figure 3. **Surface representation of N*bcRON2hp complexed with FVO *Pf*AMA1.** The MTSL spin label (cyan) of the peptide probe (orange stick) projects towards the hot spot at the centre of the cleft (green). Some hot spot forming residues flanked at one side of the druggable hot spot are highlighted in sticks in the enlarged box.

Interestingly, a cavity was formed near the base of the DII loop that overlapped partially with the druggable pocket mentioned above. The cavity is surrounded by several conserved hydrophobic residues Tyr142, Val137, Tyr234, Tyr236 and Tyr251, which also form the hot-spot identified in a computational study of the R1-3D7 *Pf*AMA1 complex structure.[38] Tyr251 is highly conserved across *Plasmodium* species and is essential to the AMA1-RON2 interaction.[16] Furthermore, recent computational and biophysical studies of the AMA1-RON2 interaction have suggested the importance of the aromatic subsite (Tyr142, Tyr234, Tyr236 and Tyr251) for binding of a non-peptide inhibitor.[39] Our structure showed that the spin label is well positioned to confer PRE on any small molecules binding to this druggable pocket in the cleft.

The highly flexible and dynamic DII loop, which is absent in the *apo* FVO *Pf*AMA1 structures (PDB id: 4R1A)[40] and its complex with RON2hp analogues (PDB id: 4Z0D, 4Z0E, 4Z0F, 4Z09),[31] was partly resolved in this structure in a new conformation (Figure 4).

Most of the residues in the DII loop (residues 350-388) were resolved in the electron density except residues 354-359 and 385-387. As the DII loop is conserved in both 3D7 and FVO *Pf*AMA1, the DII loop conformation in this structure was compared with the reported DII loop in *apo* (PDB: 1Z40)[41] and IgNAR-bound 3D7 *Pf*AMA1 (PDB: 2Z8V),[42] in which the complete DII loop is modelled. In both the *apo* and IgNAR-bound 3D7 *Pf*AMA1 structures, the DII loop is resolved in a similar conformation that covers much of the functional binding site. The 360-367 segment is helical in all structures but is displaced outward from the DI surface in the N*bcRON2hp-FVO *Pf*AMA1 complex structure, rather than packing against that surface as it does in the 3D7 structures (Figures 4 and S4). Residues 370-379 form the hairpin tip of DII that covers the hydrophobic pocket in the 3D7 structures but are helical in the N*bcRON2hp-FVO *Pf*AMA1 complex. This conformational change exposes the hydrophobic pocket in a partially open gap mediated by the DII hairpin and flexible Ib loop.[42] The position of the Ib loop is not resolved in the *apo*[36] and complex structures of FVO *Pf*AMA1,[31] but is stabilised by polar interactions between Thr171 and Gln174 and resolved in electron density. Thus, binding of the spin-labelled peptide to FVO *Pf*AMA1 induced displacement of the loops that cover the pocket, exposing the pocket to solvent for small molecule binding, and is therefore suitable to test compounds in the presence of the probe for PRE.

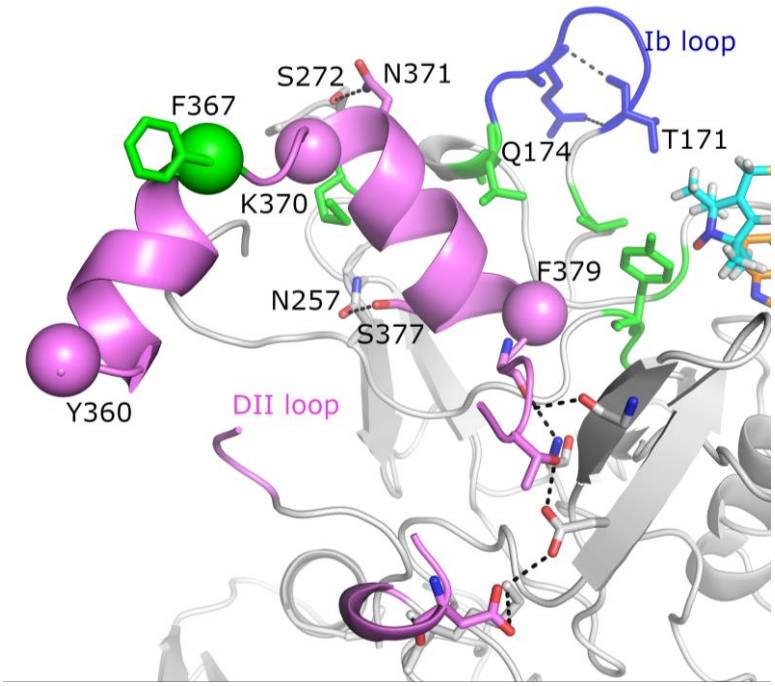

Figure 4. **DII loop conformation**. The DII loop is resolved in new conformation with most of the residues in density. Polar interactions between side chains of Ser377 and Asn257, and Asn371 and Ser272 stabilise the 370-379 segment as a helix. The 360-367 helix projects outward from the surface. Residues at the limits of the defined segments are indicated by sphere. Green sticks represent hydrophobic residues and domain Ib loop in blue.

Crystal packing against the DII loop showed that N*bcRON2hp from a neighbouring protein is stabilising the 360-367 helix through inter-chain contacts, which might explain the resolved conformation of this segment (Figure S5). Residues 370-379, including the hairpin of DII, were resolved as a helix that is stabilised by polar interactions between Asn371 and Ser272, and Ser377 and Asn257 (Figure 4). Polar contacts mediated by Asp134 and Thr382, the main chain of Leu380 [O] and Arg143 [N] may also contribute to its stabilisation. Alternatively, this new structure may represent an intermediate conformation in the displacement of the highly dynamic DII loop from the RON2 binding site, as suggested recently by Delgadillo *et al*.[43]

PRE-based screening of compounds

To assess the utility of the designed probe N*bcRON2hp for PRE, six fragments were tested individually in the presence of the probe (Figure 5). The selected compounds represent five different scaffolds among the 57 hits that were positive in both saturation transfer difference (STD) and Carr-Purcell-Meiboom-Gill (CPMG) experiments and whose binding was competed by the R1 peptide.[18] We also tested a representative of the pyrrolo pyrimidine scaffold (**6**) for which the binding site on AMA1 is unknown.[44] We observed PRE conferred by the spin-label on the spectra of these compounds, which are in fast exchange between the free and bound states, effectively a transferred PRE. We observed transverse relaxation (T_2) by recording their one-dimensional ^{1}H NMR spectra using CPMG at various spin lock periods (0-300 ms). The sub-stoichiometric concentration of the spin-labelled probe (1:3 probe to protein ratio) was chosen in the screen to minimize any false positives arising from non-specific binding of the probe to AMA1. The concentration of the fragment hits was limited to 5-fold higher than the protein concentration so that the PRE was not compromised by slowly-relaxing signals from excess ligands that were not affected by the protein-bound spin label.

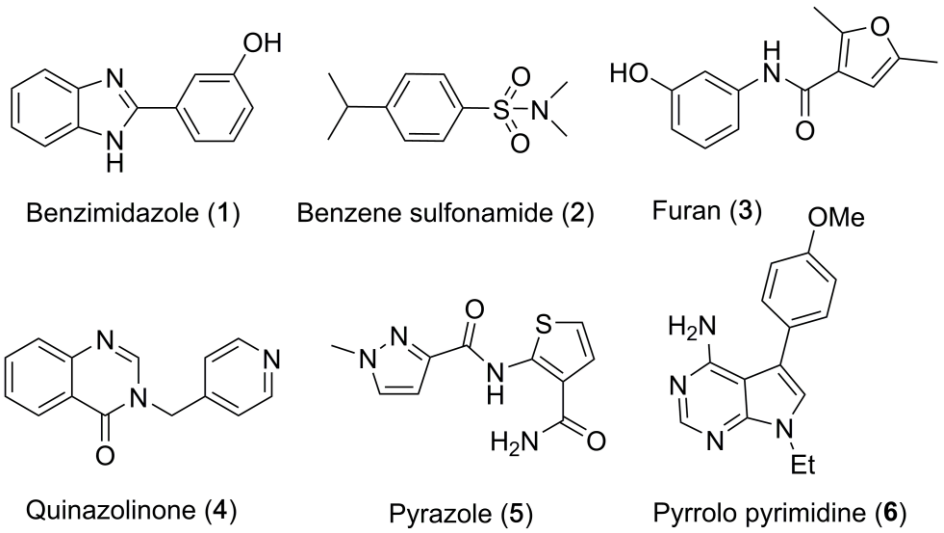

Figure 5. Fragment hits from representative scaffold series screened in the presence of N*bcRON2hp and AMA1.

The transverse relaxation profile of benzimidazole (**1**) is illustrated in Figures 6 and S6. In the free state, **1** is expected to rotate quickly, relax slowly and yield sharp signals (data not shown). Upon binding to AMA1, the compound tumbled slowly, resulting in faster relaxation and therefore line broadening (Figures 6A, S6). After addition of N*bcRON2hp, further broadening of signals was observed; some peaks broadened beyond detection at a spin-lock time of 150 ms (eg. H4) and all resonances disappeared at 300 ms (Figures 6A, orange vs blue, S6).

Upon reduction of the paramagnetic nitroxide to the diamagnetic state by addition of ascorbate, the signals recovered in intensity (Figure 6B, green vs orange). Peak recovery was also obvious in spectra recorded in the presence of diamagnetic A_bcRONhp peptide (Figure 6C, black vs orange). This clearly indicated that the enhanced relaxation of proton signals after adding the spin-label was due to PRE conferred by the oxidised spin.

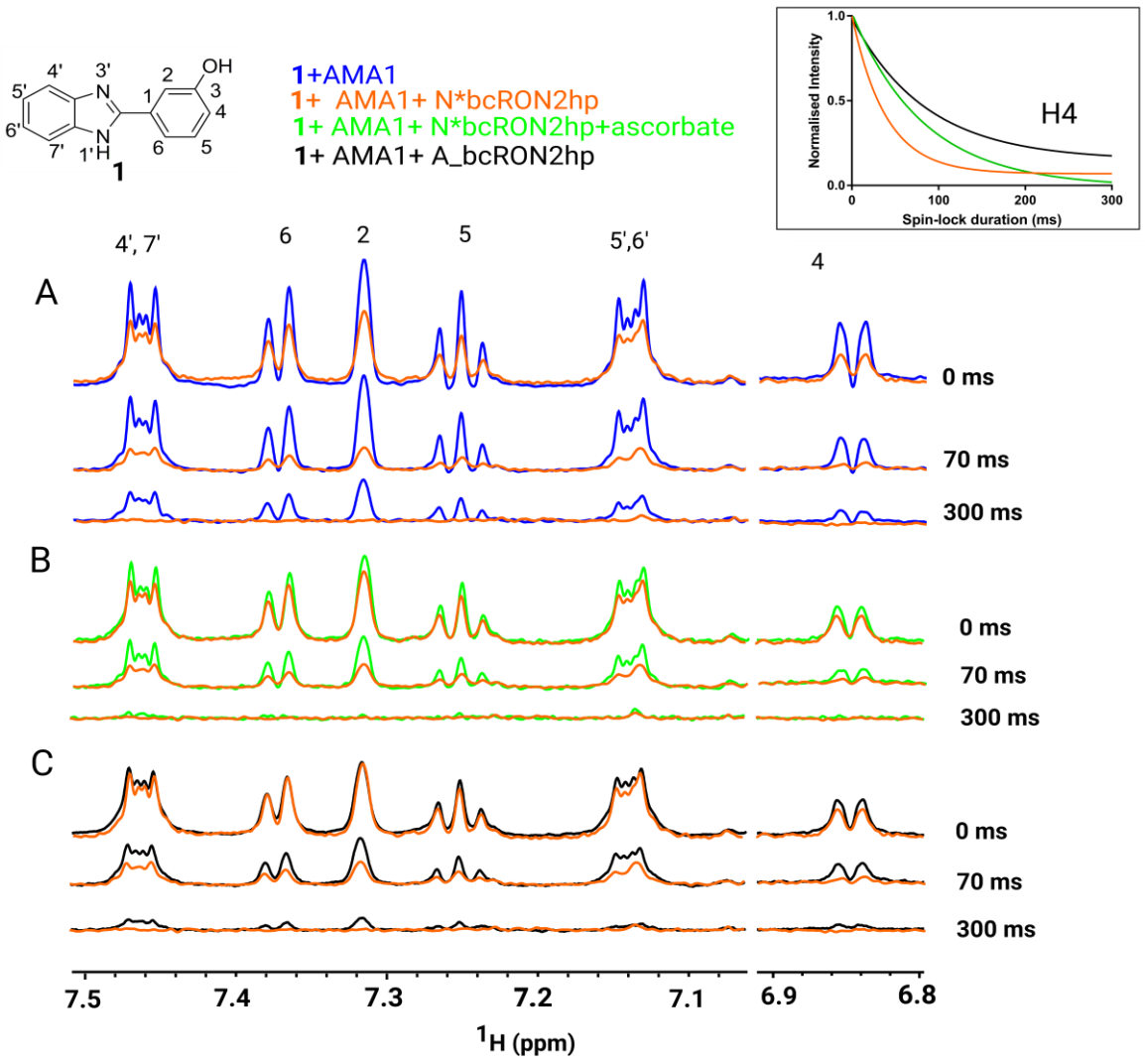

Figure 6. **PRE based screening of benzimidazole (1).** A. CPMG spectra are shown at spin-lock periods of 0, 70 and 300 ms. AMA1-bound fragment signal (blue) is broadened in the presence of N*bcRON2hp (orange) owing to PRE. B. Recovery of signals upon reduction of the paramagnetic nitroxide to the diamagnetic state by ascorbate (green vs orange) and C. in a separate study with the peptide without the spin-label, A_bcRON2hp (black vs orange). The concentrations used in each experiment were 50 µM **1**, 10 µM *Pf*AMA1 FVO, 3 µM N*bcRON2hp and 3 µM A_bcRON2hp. Spectra were acquired at 10 °C with 128 scans. The inset shows best fit to a single exponential for paramagnetic (orange) and diamagnetic (green and black represent ascorbate and A_bcRON2hp, respectively) samples by least squares method using Prism. Enhanced relaxation of proton H4 in the paramagnetic state slowed down upon conversion to the diamagnetic state.

Complete broadening of resonances from all proton signals of the benzene sulfonamide (**2**) (Figure 7), furan (**3**), quinazolinone (**4**), pyrazole (**5**), and pyrrolo pyrimidine (**6**) at 300 ms in the presence of the spin-labelled peptide was also observed (Figure S7). These results suggested that all of these compounds bind to similar binding sites in the hydrophobic cleft,

including compound **6**, for which the binding site was previously unknown. When the nitroxide was quenched by ascorbate reduction, all fully broadened peak intensity was partially recovered, confirming that the enhanced relaxation was caused by the unpaired electron's effect on the protons (Figure 7B, green vs. orange and S7). It is unclear to us why the broadened signals did not recover their full intensity in the reduced spin state. One explanation could be that the ascorbate failed to reduce the nitroxide tag fully to the diamagnetic hydroxylamine owing to the slightly hydrophobic environment in the bound state and ascorbate radical reoxidised the hydroxylamine back to nitroxide, causing slow exchange of the diamagnetic to the paramagnetic state.[29]

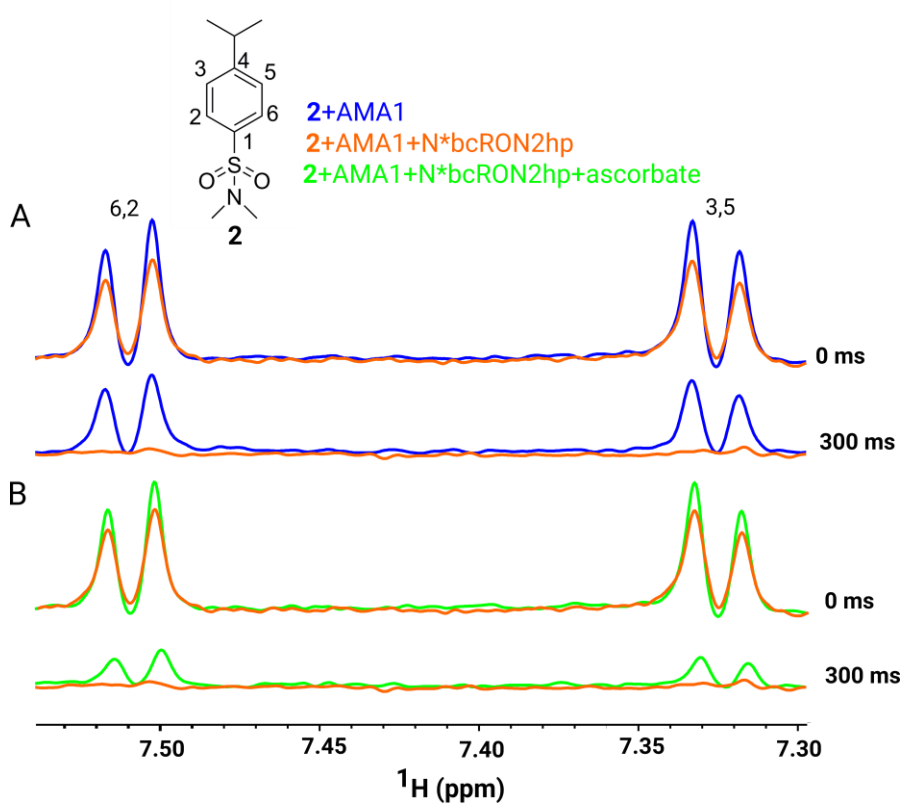

Figure 7. NMR profile of benzene sulfonamide (2) in PRE-based screening. A. CPMG spectra are shown at spin-lock periods of 0 and 300 ms. AMA1-bound fragment signal (blue) is broadened in the presence of N*bcRON2hp (orange) owing to PRE. B. Recovery of signals upon reduction of the paramagnetic nitroxide to the diamagnetic state by ascorbate (green vs orange). Spectra were acquired at 10 °C with 128 scans. Concentrations of **2**, N*bcRON2hp and AMA1 were 50, 3 and 10 µM, respectively.

We attempted to assess the PRE rate (Γ_2) by measuring the difference in transverse relaxation rates between the paramagnetic ($R_{2,\ para}$) and diamagnetic ($R_{2,\ dia}$) states of the probe using the equation $\Gamma_2 = R_{2,\ para} - R_{2,\ dia}$.[45] As we acquired CPMG spectra, which

measure relaxation in the transverse plane (T_2 relaxation), for both paramagnetic and diamagnetic samples, this subtraction cancels out relaxation mechanisms common to both states, such that the only remaining relaxation mechanism arises from electron-nucleus interactions (i.e., the PRE effect). The effects of conformational exchange and internal motion on relaxation, therefore, do not contribute. PRE effects were analysed for each individual proton in **1**. Protons from different parts of **1** showed different PRE magnitudes, presumably as a consequence of the relative orientation of the compound to the spin-label. The protons around the phenolic ring experienced stronger PRE effects than those on the benzimidazole ring, suggesting orientation of the phenolic ring towards the spin label (Figure S8, Table S1).

We conducted several control experiments to validate the PRE effects. The above CPMG experiments were conducted similarly on compounds in the presence of N*bcRON2hp peptide but no AMA1. As expected, no paramagnetic enhancement was detected after adding the spin label, and the resulting spectra were identical to those of the free compounds, as exemplified by **1** (Figure S9). This demonstrated that there was no direct interaction between the probe and **1**, and the PRE effects observed above were due entirely to simultaneous binding of the probe and compounds to AMA1, which brought those molecules into spatial proximity. Another CPMG control study was performed on an AMA1 non-binder, dopamine (**7**), as a negative control. The resonances of **7** in the presence of AMA1 were similar to those observed after adding N*bcRON2hp (Figure S10), confirming that the PRE effects observed with **1-6** were due to the binding of these molecules in close proximity to the spin-label.

Along with the CPMG control studies, a separate STD study was performed to assess if compound binding to AMA1 was affected in the presence of N*bcRON2hp. STD signals of the fragments were identical before and after addition of the diamagnetic A_bcRON2hp, as illustrated for benzimidazole (**1**) in figure S11, indicating that the fragments bound to the cleft other than the probe binding site, and thus, the probe did not interfere with the binding sites for this diverse range of fragments.

We tried to measure quantitative PRE effects conferred by N*bcRON2hp on amide groups of ^{15}N-labelled AMA1 for any non-specific binding of the probe. However, this analysis was complicated by intermediate exchange broadening of the peaks in the bound state of the peptide at the tested concentration.

Conclusion

A spin-labelled probe was successfully designed based on RON2. The binding mode of the probe and the position of the spin label were defined in a crystal structure of the probe complexed with FVO *Pf*AMA1. The probe bound to AMA1 at one end of the cleft such that the spin label was oriented towards the centre of the hydrophobic cleft, thereby making it suitable for conferring PRE on small molecules binding to the druggable hydrophobic pocket. PRE-based screening along with several control studies indicated that the ligand binding sites were distinct from but close to (~20 Å) the probe binding site and experienced different degrees of PRE effects according to their orientation. The probe enabled us to better define the binding site(s) of the small molecules in the context of the broader hydrophobic groove of AMA1. This simple and straightforward qualitative assessment of PRE effects is applicable for screening of compounds and to obtain general information on the binding site in the broad shallow binding surface of a dynamic system like AMA1. Quantitative PRE measurements will be extended to derive distance- and orientation-dependent positional constraints of the small molecule ligands to direct subsequent ligand optimisation.

Experimental Section

Protein preparation

Constructs incorporating domains I and II of the ectodomains of 3D7 and FVO *Pf*AMA1 (residues 104-438) were expressed in *Escherichia coli* BL21 (DE3) as *N*-terminal His-tagged proteins in the pPROEX HTb vector, purified and refolded according to the previously published protocol.[18] Details are presented in the Supporting Information.

Synthesis and purification of the spin-labelled peptide probe

All peptides were synthesised on a 0.1 mmol scale using standard Fmoc-based solid-phase peptide synthesis on a PS3 (Protein Technologies Inc.) automated solid-phase peptide synthesiser. For the spin-labelled peptide N*bcRON2hp, the backbone-cyclised peptide, bcRON2hp was first synthesised from its precursor linear peptide. The first amino acid was loaded on to the 2-chlorotrityl chloride resin (1.2 mmol/g) manually in the presence of 6 eq of diisopropylethylamine (DIPEA) in dichloromethane (DCM). The unreactive sites on the resin were capped with a freshly-prepared solution mixture of DCM: MeOH: DIPEA (17:2:1). Other amino acids were attached following standard Fmoc-deprotection and coupling using a

3-fold excess of *O*-(1*H*-6-chlorobenzotriazole-1-yl)-1,1,3,3-tetramethyluronium hexafluorophosphate (HCTU) as coupling agent, in the presence of DIPEA in *N*,*N*-dimethylformamide (DMF). The peptide with protected side chains was cleaved off the resin with 1% TFA in DCM, precipitated with cold diethyl ether (Et_2O), dried in *vacuo*, and lyophilised. For backbone cyclisation, the crude linear peptide was dissolved (1 mg/mL) in a mixture of 3 eq of the coupling reagent (6-chlorobenzotriazol-1-yloxy)-tripyrrolidinophosphonium hexafluorophosphate (PyClocK) and 10 eq of DIPEA in DMF and stirred continuously at 25 °C for 20 h. The side-chain protecting groups were removed using a mixture of TFA/thioanisole/phenol/water/DODT (82.5/5/5/5/2.5). The crude peptide was precipitated with cold Et_2O and dissolved in 20% acetonitrile before lyophilisation. The peptide was purified by reverse-phase HPLC on a Vydac 218 TP C18 column (250 × 10 mm, 10 μm). Peptide purity (100%) and molecular mass (*m*/*z* $[M+H]^+$ calcd: 1529.9, found: 1530.7) were checked by electrospray ionisation LC-MS.

For N*bcRON2hp, MTSL (*S*-(1-oxyl-2,2,5,5-tetramethyl-2,5-dihydro-1H-pyrrol-3-yl) methyl methanesulfonothioate) (Adipogen Life Sciences) was added to a 0.2 mM solution of bcRON2hp (Cys2037-D-Pro2049 cyclised) in 20 mM Tris-HCl, pH 7 from a freshly prepared stock (150 mM in MeOH) and reacted for 2 h at 25 °C under N_2 in the dark. Upon completion of the reaction, peptide was purified directly by preparative HPLC using the same column as above. The purity (>95%) and molecular mass of the labelled peptide (*m*/*z* $[M+H]^+$ calcd: 1714.3, found: 1714.7) were verified by LC-MS. Details of the purification protocol are given in the Supporting Information.

The free thiol of Cys2037 of the unlabelled bcRON2hp peptide (Cys2037-D-Pro2049 cyclised) was alkylated by adding equimolar iodoacetamide from freshly prepared stock (87 mM in 100 mM NH_4HCO_3) to 0.5 mM peptide in 100 mM NH_4HCO_3 and reacted for 3 h in the dark at 25 °C. The alkylated peptide, A_bcRON2hp was purified similarly to bcRON2hp and authenticated by LC-MS for molecular mass (*m*/*z* $[M+H]^+$ calcd: 1586.83, found: 1586.78) and purity 100%.

Surface plasmon resonance binding analysis

The binding affinities of the peptides for 3D7 *Pf*AMA1$_{104-438}$ and FVO *Pf*AMA1$_{104-438}$ were analysed using a Biacore T200 biosensor instrument (GE Healthcare). Proteins were immobilised onto a CM5 chip (GE Healthcare) using a standard amide coupling protocol according to the manufacturer's instructions to achieve a target level of 2000 RU. SPR

experiments were performed at 25 °C using HBS-EP (10 mM HEPES, 150 mM NaCl, 0.1% EDTA and 0.05% surfactant P20, pH 7.4) as the running buffer. Peptide stocks were prepared in water (1 mg/mL) and diluted in fresh running buffer immediately before the run. To generate binding data, peptides were injected over immobilised AMA1 at concentrations ranging from 0.1 to 100 μM at a constant flow rate of 90 μL/min for 30 s. Peptide dissociation was monitored by flowing running buffer at 90 μL/min for 120 s. Bulk refractive index changes were eliminated by subtracting the reference flow cell responses. Dissociation constants (K_D) were determined by fitting to a steady-state affinity model using Biacore T200 evaluation software.

Electron paramagnetic resonance measurements

X-band continuous-wave electron paramagnetic resonance (EPR) spectra were acquired on a Bruker Elexsys E500 spectrometer fitted with a Bruker super-high-Q probehead (ER 4122SHQE). The microwave power was set to 20 mW and the magnetic field was modulated at 100 kHz with an amplitude of 1 G. Samples (120 μL) were placed in a quartz flat cell (Wilmad, WG-808-Q) and spectra were recorded at 25 °C over 100 G at a rate of 1 G/s. The receiver gain was set 70 dB with time constant of 164 ms. All samples were prepared in 20 mM Tris-HCl buffer, pH 8, at peptide and protein concentrations of 10 and 15 μM, respectively. EPR spectra of both N*bcRONhp and bcRON2hp were acquired in the presence and absence of FVO *Pf*AMA1, where bcRON2hp served as diamagnetic control. Spectral simulations were performed using the Easyspin v.4.5.5 software suite on MATLAB.[46]

Crystallization, data collection, structure solution and refinement

For crystallography studies with bcRON2hp and N*bcRON2hp, the FVO *Pf*AMA1-peptide complex was concentrated to 6 and 8 mg/mL respectively. Crystals of the complex were obtained by the hanging drop method in 15-20% PEG400, 0.1 M Tris pH 8.4, 20% isopropanol and 0.1 M sodium acetate. Single crystals were flash-cooled in liquid nitrogen. Diffraction data were collected at 100 K using synchrotron radiation on the MX1 beamline (3BM1) at the Australian synchrotron. Data were processed using XDS[47] and scaled using AIMLESS[48] from the CCP4 suite.[49] Crystallographic parameters and data collection statistics are provided in Table 2. Initial phases were obtained by the molecular replacement method using the program PHASER[50] and chain A of PDB id 4R1A as a search model.[40] Model building and structural validation were performed using Phenix[51] and Coot.[52] The coordinates and structure factors are available from the Protein Data Bank[53] (entry 6N7Q

and 6N87). All structure figures were prepared in the PyMOL Molecular Graphics System, version 1.3r2 (Schrödinger, LLC).

NMR measurements

For PRE-based screening experiments, fragments were diluted from their concentrated stocks (200 mM in $^{2}H_6$-DMSO) in 20 mM phosphate buffer, pH 6.8, containing 10% $^{2}H_2O$ and 1% $^{2}H_6$-DMSO to give a final concentration of 50 µM. In each experiment, FVO *Pf*AMA1, and peptides either spin-labelled N*bcRON2hp or, unlabelled A_bcRON2hp were used at 10 and 3 µM, respectively. For reduction of the N*bcRON2hp, a 30-fold molar excess of sodium ascorbate was added from freshly prepared buffered concentrated stock, and the samples were kept at 35 °C for 1 h, followed by overnight incubation at 4 °C.

All NMR experiments were conducted on a Bruker Avance III 600 MHz spectrometer equipped with a TXI-cryoprobe. One representative elaborated fragment from each of five diverse scaffolds of *Pf*AMA1 hits[18] was rescreened by CPMG experiments performed at 10 °C with 128 scans, with presaturation to suppress the residual water peak. The CPMG reference spectra of the free and *Pf*AMA1-bound fragments were acquired with a constant spin echo delay of 1 ms and spin-lock periods of 0, 10, 30, 50, 70, 100, 150, 200 and 300 ms. The same sets of experiments were carried out on N*bcRONhp added to the *Pf*AMA1-bound fragment samples, both before and after reduction of the spin label by ascorbate. The signal intensity of different CPMG experiments was normalised by using the intensity at 0 ms spin-lock time and the relaxation data were fitted to single exponentials by non-linear, least-squares curve fitting using GraphPad Prism 7 software to obtain transverse relaxation rates (R_2). CPMG control experiments were performed at the same experimental settings using A_bcRON2h as a diamagnetic reference. Similarly, another CPMG control was conducted on free fragment samples before and after adding N*bcRON2hp. CPMG spectra of a non-binder of *Pf*AMA1 served as negative control for PRE.

Binding of fragments to *Pf*AMA1 in the presence of N*bcRON2hp was examined by acquiring STD spectra before and after adding A_bcRON2hp. Parameters were kept identical to the initial STD screen.[18] Saturation was achieved by a 5 s train of 50 ms Gaussian pulses, with the irradiation frequency of the saturation pulse train changed after every scan (on- and off-resonance frequencies were -380 and -20000 Hz, respectively). Spectra were recorded at 10 °C with total 2048 scans. All spectra were processed and analysed in Topspin3.7.

Acknowledgements

This work was supported in part by an Australian National Health and Medical Research Council (NHMRC) project grant (1098884). R. S. N. acknowledges fellowship support from the NHMRC. We thank the Australian Synchrotron for beam-time and technical assistance. S.C.D. was supported by a fellowship awarded by the faculty of Medicine, Dentistry and Health Sciences, The University of Melbourne.

Keywords: AMA1• drug discovery • malaria• NMR spectroscopy • spin label

Abbreviations: AMA1 apical membrane antigen 1, RON2 rhoptry neck protein, EPR electron paramagnetic resonance, PRE paramagnetic relaxation enhancement, STD saturation transfer difference, CPMG Carr-Purcell-Meiboom Gill

Crystallographic data deposited in the Protein Data Bank under PDB ID 6N7Q and 6N87 will be released upon publication

References

[1] WHO, Global Report on Insecticide Resistance in Malaria Vectors: 2010–2016, **2018**.

[2] WHO,World Malaria Report 2016, **2017**.

[3] M. Imwong, A. M. Dondorp, F. Nosten, P. Yi, M. Mungthin, S. Hanchana, D. Das, A. P. Phyo, K. M. Lwin, S. Pukrittayakamee, et al., *Antimicrob. Agents Chemother.* **2010**, *54*, 2886–2892.

[4] F. Ariey, B. Witkowski, C. Amaratunga, J. Beghain, A.-C. Langlois, N. Khim, S. Kim, V. Duru, C. Bouchier, L. Ma, et al., *Nature* **2014**, *505*, 50–55.

[5] C. Amaratunga, P. Lim, S. Suon, S. Sreng, S. Mao, C. Sopha, B. Sam, D. Dek, V. Try, R. Amato, et al., *Lancet Infect. Dis.* **2016**, *16*, 357–365.

[6] R. Leang, W. R. J. Taylor, D. M. Bouth, L. Song, J. Tarning, M. C. Char, S. Kim, B. Witkowski, V. Duru, A. Domergue, et al., *Antimicrob. Agents Chemother.* **2015**, *59*, 4719–4726.

[7] WHO, *Status Report on Artemisinin and ACT Resistance (April 2017)*, **2017**.

[8] A. T. Bright, E. A. Winzeler, *Nature* **2013**, *498*, 446–447.

[9] L. D. Sibley, *Curr. Opin. Biotechnol.* **2010**, *21*, 592–598.

[10] M. Lamarque, S. Besteiro, J. Papoin, M. Roques, B. Vulliez-Le Normand, J. Morlon-Guyot, J.-F. Dubremetz, S. Fauquenoy, S. Tomavo, B. W. Faber, et al., *PLoS Pathog.* **2011**, *7*, e1001276.

[11] J. S. Tyler, J. C. Boothroyd, *PLOS Pathog.* **2011**, *7*, e1001282.

[12] D. Richard, C. A. MacRaild, D. T. Riglar, J.-A. Chan, M. Foley, J. Baum, S. A. Ralph, R. S. Norton, A. F. Cowman, *J. Biol. Chem.* **2010**, *285*, 14815–14822.

[13] P. Srinivasan, A. Yasgar, D. K. Luci, W. L. Beatty, X. Hu, J. Andersen, D. L. Narum, J. K. Moch, H. Sun, J. D. Haynes, et al., *Nat. Commun.* **2013**, *4*, 2261.

[14] C. R. Collins, C. Withers-Martinez, G. A. Bentley, A. H. Batchelor, A. W. Thomas, M. J. Blackman, *J. Biol. Chem.* **2007**, *282*, 7431–7441.

[15] D. T. Riglar, D. Richard, D. W. Wilson, M. J. Boyle, C. Dekiwadia, L. Turnbull, F. Angrisano, D. S. Marapana, K. L. Rogers, C. B. Whitchurch, et al., *Cell Host Microbe* **2011**, *9*, 9–20.

[16] C. R. Collins, C. Withers-Martinez, F. Hackett, M. J. Blackman, *PLoS Pathog.* **2009**, *5*, e1000273.

[17] S. M. Devine, C. A. MacRaild, R. S. Norton, P. J. Scammells, *Med. Chem. Commun.* **2017**, *8*, 13–20.

[18] S. S. Lim, C. O. Debono, C. A. MacRaild, I. R. Chandrashekaran, O. Dolezal, R. F. Anders, J. S. Simpson, M. J. Scanlon, S. M. Devine, P. J. Scammells, et al., *Aust. J. Chem.* **2013**, *66*, 1530–1536.

[19] B. Krishnarjuna, S. S. Lim, S. M. Devine, C. O. Debono, R. Lam, I. R. Chandrashekaran, G. Jaipuria, H. Yagi, H. S. Atreya, M. J. Scanlon, et al., *J. Mol. Recognit.* **2016**, *29*, 281–291.

[20] S. M. Devine, M. D. Mulcair, C. O. Debono, E. W. W. Leung, J. W. M. Nissink, S. S. Lim, I. R. Chandrashekaran, M. Vazirani, B. Mohanty, J. S. Simpson, et al., *J. Med. Chem.* **2015**, *58*, 1205–1214.

[21] X. Ge, C. A. MacRaild, S. M. Devine, C. O. Debono, G. Wang, P. J. Scammells, M. J. Scanlon, R. F. Anders, M. Foley, R. S. Norton, *J. Med. Chem.* **2014**, *57*, 6419–6427.

[22] I. Solomon, *Phys. Rev.* **1955**, *99*, 559–565.

[23] N. Bloembergen, L. O. Morgan, *J. Chem. Phys.* **1961**, *34*, 842–850.

[24] K. Sale, L. Song, Y.-S. Liu, E. Perozo, P. Fajer, *J. Am. Chem. Soc.* **2005**, *127*, 9334–9335.

[25] W. L. Hubbell, C. J. Lopez, C. Altenbach, Z. Yang, *Curr. Opin. Struct. Biol.* **2013**, *23*, 725–733.

[26] P. A. Kosen, *Methods Enzymol.* **1989**, *177*, 86–121.

[27] J. R. Gillespie, D. Shortle, *J. Mol. Biol.* **1997**, *268*, 170–84.

[28] J. R. Gillespie, D. Shortle, *J. Mol. Biol.* **1997**, *268*, 158–169.

[29] Y. Xue, I. S. Podkorytov, D. K. Rao, N. Benjamin, H. Sun, N. R. Skrynnikov, *Protein Sci.* **2009**, *18*, 1401–1424.

[30] W. Jahnke, L. B. Perez, C. G. Paris, A. Strauss, G. Fendrich, C. M. Nalin, *J. Am. Chem. Soc.* **2000**, *122*, 7394–7395.

[31] G. Wang, N. Drinkwater, D. R. Drew, C. A. MacRaild, D. K. Chalmers, B. Mohanty, S. S. Lim, R. F. Anders, J. G. Beeson, P. E. Thompson, et al., *J. Mol. Biol.* **2016**, *428*, 3986–3998.

[32] G. Wang, C. A. Macraild, B. Mohanty, M. Mobli, N. P. Cowieson, R. F. Anders, J. S. Simpson, S. Mcgowan, R. S. Norton, M. J. Scanlon, **2014**, *9*, 1–12.

[33] P. Srinivasan, W. L. Beatty, A. Diouf, R. Herrera, X. Ambroggio, J. K. Moch, J. S. Tyler, D. L. Narum, S. K. Pierce, J. C. Boothroyd, et al., *Proc. Natl. Acad. Sci. U. S. A.* **2011**, *108*, 13275–13280.

[34] Wang Geqing, PhD thesis, Monash University (AU), **2015**;

[35] B. Vulliez-Le Normand, M. L. Tonkin, M. H. Lamarque, S. Langer, S. Hoos, M. Roques, F. A. Saul, B. W. Faber, G. A. Bentley, M. J. Boulanger, et al., *PLoS Pathog.* **2012**, *8*, DOI 10.1371/journal.ppat.1002755.

[36] G. Marius Clore, J. Iwahara, *Chem. Rev.* **2009**, *109*, 4108–4139.

[37] C. A. Macraild, R. F. Anders, M. Foley, R. S. Norton, *Curr. Top. Med. Chem.* **2011**, *11*, 2039–2047.

[38] G. Wang, C. A. MacRaild, B. Mohanty, M. Mobli, N. P. Cowieson, R. F. Anders, J. S. Simpson, S. McGowan, R. S. Norton, M. J. Scanlon, *PLoS One* **2014**, *9*, 1–12.

[39] E. Pihan, R. F. Delgadillo, M. L. Tonkin, M. Pugniere, M. Lebrun, M. J. Boulanger, D. Douguet, *J. Comput. Aided. Mol. Des.* **2015**, *29*, 525–539.

[40] S. S. Lim, W. Yang, B. Krishnarjuna, K. Kannan Sivaraman, I. R. Chandrashekaran, I. Kass, C. A. Macraild, S. M. Devine, C. O. Debono, R. F. Anders, et al., *Biochemistry* **2014**, *53*, 7310–20.

[41] T. Bai, M. Becker, A. Gupta, P. Strike, V. J. Murphy, R. F. Anders, A. H. Batchelor, *Proc. Natl. Acad. Sci. U. S. A.* **2005**, *102*, 12736–12741.

[42] K. A. Henderson, V. A. Streltsov, A. M. Coley, O. Dolezal, P. J. Hudson, A. H. Batchelor, A. Gupta, T. Bai, V. J. Murphy, R. F. Anders, et al., *Structure* **2007**, *15*, 1452–1466.

[43] R. F. Delgadillo, M. L. Parker, M. Lebrun, M. J. Boulanger, D. Douguet, *PLoS One* **2016**, *11*, 1–20.

[44] S. M. Devine, S. S. Lim, I. R. Chandrashekaran, C. A. MacRaild, D. R. Drew, C. O. Debono, R. Lam, R. F. Anders, J. G. Beeson, M. J. Scanlon, et al., *Med. Chem. Commun.* **2014**, *5*, 1500–1506.

[45] J. Iwahara, C. Tang, G. Marius Clore, *J. Magn. Reson.* **2007**, *184*, 185–195.

[46] S. Stoll, A. Schweiger, *J. Magn. Reson.* **2006**, *178*, 42–55.

[47] W. Kabsch, *Acta Crystallogr. Sect. D Biol. Crystallogr.* **2010**, *66*, 125–132.

[48] P. R. Evans, *Acta Crystallogr. Sect. D Biol. Crystallogr.* **2011**, *67*, 282–292.

[49] M. D. Winn, *J. Synchrotron Radiat.* **2003**, *10*, 23–25.

[50] A. J. McCoy, R. W. Grosse-Kunstleve, L. C. Storoni, R. J. Read, *Acta Crystallogr. Sect. D Biol. Crystallogr.* **2005**, *61*, 458–464.

[51] P. D. Adams, P. V. Afonine, G. Bunkóczi, V. B. Chen, I. W. Davis, N. Echols, J. J. Headd, L. W. Hung, G. J. Kapral, R. W. Grosse-Kunstleve, et al., *Acta Crystallogr. Sect. D Biol. Crystallogr.* **2010**, *66*, 213–221.

[52] P. Emsley, K. Cowtan, *Acta Crystallogr. Sect. D Biol. Crystallogr.* **2004**, *60*, 2126–2132.

[53] H. M. Berman, J. Westbrook, Z. Feng, G. Gilliland, T. N. Bhat, H. Weissig, I. N. Shindyalov, P. E. Bourne, *Nucleic Acids Res.* **2000**, *28*, 235–242.